Characterization of the ground X 1 state of 204 Pb 19 F, 206 Pb 19 F, 207 Pb 19 F, and 208 Pb 19 F

Article *in* Physical Review A · August 2011

DOI: 10.1103/PHYSREVA.84.022508

Characterization of the ground X_1 state of $^{204}Pb^{19}F$, $^{206}Pb^{19}F$, $^{207}Pb^{19}F$, and $^{208}Pb^{19}F$

Richard J. Mawhorter, Benjamin S. Murphy, and Alexander L. Baum
Department of Physics and Astronomy, Pomona College, Claremont, California 91711-6327, USA

Trevor J. Sears
Chemistry Department, Brookhaven National Laboratory, Upton, New York 11973-5000, USA

T. Yang, P. M Rupasinghe, C. P. McRaven, and N. E. Shafer-Ray
Homer L. Dodge Department of Physics and Astronomy, University of Oklahoma, Norman, Oklahoma, USA

Lukas D. Alphei and Jens-Uwe Grabow
Gottfried-Wilhelm-Leibniz-Universität, Institut für Physikalische Chemie & Elektrochemie, Lehrgebiet A, D-30167 Hannover, Germany
(Received 12 March 2011; published 17 August 2011)

Pure rotational spectra of the ground electronic-vibrational X_1 state of $^{204}Pb^{19}F$, $^{206}Pb^{19}F$, $^{207}Pb^{19}F$, and $^{208}Pb^{19}F$ are measured with a resonator pulsed supersonic jet Fourier-transform microwave spectrometer. Also reported is a new measurement of the Stark effect on the optical spectra of $A \leftarrow X_1$ transitions. These spectra are combined with published high-resolution infrared spectra of $X_2 \leftrightarrow X_1$ transitions in order to create a complete picture of the ground state of lead monofluoride. For the microwave data, molecules are prepared by laser ablation of lead target rods and stabilized in a supersonic jet of neon mixed with sulfur hexafluoride. For the optical Stark spectra, a continuous source of molecules is created in a nozzle heated to 1000 °C. The microwave spectra confirm, improve, and extend previously reported constants that describe the rotational, spin-orbit, and hyperfine interactions of the ground electronic state of the PbF molecule. A discrepancy concerning the sign of the hyperfine constant describing the ^{207}Pb nucleus is discussed. Magnetic-field-dependent microwave spectra are used to characterize the Zeeman interaction in terms of two g factors of the body-fixed electronic wave function. The optical Stark spectra are used to characterize the electric dipole moment of the X_1 and A states.

DOI: 10.1103/PhysRevA.84.022508 PACS number(s): 33.15.Mt, 31.15.aj, 21.10.Ky, 29.90.+r

I. INTRODUCTION

In 1950 Purcell and Ramsey suggested that the electron might have an electric dipole moment proportional to its spin [1]. This hypothesis initiated an ongoing hunt for the electron's electric dipole moment (eEDM). One common method to hunt for an eEDM is to investigate the electronic structure of a heavy atom or molecule in a uniform electric field that is alternately parallel and antiparallel to an applied magnetic field. Normally the energy between two states that differ only by M_F, the projection of the total total angular momentum onto the field axis, is independent of the relative direction of the fields. A nonzero eEDM would cause a small difference in this energy for the parallel and antiparallel configuration. The current limit on the electric dipole moment of 1.6×10^{-27} e cm has been determined by analyzing the energy difference between the $M_F = 1$ and $M_F = -1$ states of Tl $6\,^2P_{1/2}(F = 1)$ atoms in a $\sim$100 kV/cm field that is alternately parallel and antiparallel to a magnetic field of order 1 G [2].

In recent years, many groups have reported experiments that exploit the sensitivity of heavy diatomic molecules to an eEDM [3–8]. The large dipole moment, strong internal electric field, and small sensitivity to external magnetic fields have made the lead monofluoride molecule a leading candidate for the measurement of the electron's electric dipole moment [9–16]. As a $^2\Pi_{1/2}$ molecule, the contribution to the magnetic moment of PbF due to the electronic orbital angular momentum roughly cancels the contribution due to the unpaired electron spin angular momentum. For this reason, the g factor of a polarized PbF molecule is small ($g \approx 0.05$), greatly easing the requirements on the control of magnetic fields needed to carry out a precise eEDM experiment. We note that others are working on $^3\Delta_1$ states of the molecules WC [6], ThO [7], and HfF^+ [5], which exhibit similarly small g factors. However, as the ground state of a neutral molecule that is relatively easy to synthesize, $^2\Pi_{1/2}$ PbF may offer advantages over these other systems. Here we present an analysis of spectra and derived molecular constants that describe the hyperfine split spin-rotational levels of the ground state of PbF. These constants are critical to the design and interpretation of ongoing efforts to use PbF in an eEDM measurement.

II. EXPERIMENT

A. Fourier-transform microwave spectrometer

The study of the microwave spectrum was conducted in a supersonic jet. The preparation of the sample as a supersonic expansion of PbF in a noble carrier gas provides a virtually collisionless environment where the molecular properties can be determined in conditions of effective isolation [17]. The diatomic compound was synthesized *in situ* using laser ablation [18,19] (Nd:YAG, 1064 nm, 250 mJ, 20 Hz) of a rotating, elementary Pb rod in the presence of highly diluted SF_6 entrained in a noble carrier gas. Neon (4.5–6 bars) was used as the carrier gas. The PbF species were probed with the Balle-Flygare-type [20] Fourier-transform microwave (FTMW) spectrometer at the Gottfried-Wilhelm-Leibniz-Universität Hannover, which uses a coaxial arrangement of

the supersonic beam and resonator axis (a coaxially oriented beam-resonator arrangement, COBRA) [21,22]. Details of this experimental coherence technique are described elsewhere [23,24]. Briefly, a short (1-μs) microwave excitation pulse polarizes the molecular ensemble, and the subsequent free-induction decay of the oscillating macroscopic dipole moment is recorded in the time domain. After Fourier transform, the spectrum in the frequency domain is obtained, from which the resonance frequencies of the rotational transitions can be extracted as the arithmetic mean of the signal doublets arising from the Doppler effect of the jet expanding coaxially to the propagation axis of the standing wave field of the Fabry-Perot-type resonator. The accuracy of the frequency measurements for unblended lines at sufficient signal-to-noise ratio is on the order of 0.5 kHz. Transitions separated more than 6 kHz are resolvable.

B. Pseudocontinuous resonant enhanced multiphoton ionization

This apparatus is located at the University of Oklahoma and is described in detail elsewhere [15,25]. In brief, an effusive beam of PbF molecules is created by heating lead to 1000 °C (typical) in a MgF_2 nozzle. The beam is crossed with a tunable diode laser (436 nm, 7 mW) and pseudocontinuous laser radiation (6-ps pulse width, 76-MHz rep rate, 700 mW, 476 nm) produced from a solid-state pumped optical parametric oscillator. The diode laser radiation excites the $X_1(v=0) \leftrightarrow A(v=1)$ transition, whereas the pseudocontinuous laser radiation excites the $A(v=1) \leftrightarrow D(v=0) \leftrightarrow \mathrm{PbF}^+ + e^-$ transitions. The PbF^+ ions and electrons are then collected in coincidence in order to gain mass resolution. This pseudocontinuous resonant enhanced multiphoton ionization (pcREMPI) scheme combines the high sensitivity of conventional REMPI with a resolution of roughly 50 MHz.

III. ENERGY-LEVEL STRUCTURE OF THE $X_1(^2\Pi_{1/2})$ STATE OF PbF

A. Spin-rotational energy of PbF

To model the spin-rotational energy of the PbF molecule, we use the case (a) model as parametrized by Brown *et al.* [26], taking advantage of the matrix elements of the secular equation computed by Amiot *et al.* (Table II of Ref. [27]). Specifically we assume that the energy of a level of the $X_1\,^2\Pi_{1/2}$ state with rotational quantum number J and parity p_s is given by the minimum eigenvalue $U_-(J,p_s)$ of the following 2×2 matrix:

$$H_{\mathrm{rot}}[J,p_s] = \begin{pmatrix} \left[\frac{A}{2} + \left(B + \frac{\widetilde{A}_D}{2}\right)z\right] & [-B\sqrt{z}] \\ [-B\sqrt{z}] & \left[-\frac{A}{2} + \left(B - \frac{\widetilde{A}_D}{2}\right)(z+2)\right] \end{pmatrix} - \frac{1}{2}p_s(-1)^{J-1/2}\left(J+\frac{1}{2}\right)\begin{pmatrix} 0 & \left[\frac{-\sqrt{z}}{2}p_D\right] \\ \left[\frac{-\sqrt{z}}{2}p_D\right] & [p + p_D(z+2)] \end{pmatrix}$$
$$+ \begin{pmatrix} [\widetilde{A}_H z^2 - Dz(z+1)] & [2D\sqrt{z}(z+1) + \widetilde{A}_H\sqrt{z}] \\ [2D\sqrt{z}(z+1) + \widetilde{A}_H\sqrt{z}] & [-\widetilde{A}_H(z+2)^2 - D(z+1)(z+4)] \end{pmatrix}. \quad (1)$$

The higher eigenvalue $U_+(J,p_s)$ gives the energy of the $X_2\,^2\Pi_{3/2}$ state. Here $z = (J+\frac{1}{2})^2 - 1$. This secular equation is parametrized by the $^2\Pi$ fine-structure energy A, rotational constant B, fine-structure constant p, and higher-order corrections $\widetilde{A}_H$, $\widetilde{A}_D, D$, and p_D. The Brown parameters q and q_D considered by Amiot *et al.* [27] are not employed in our fits to observed transitions because they make negligible contributions to the eigenvalues. This parametrization allows us to create a global fit to both the pure rotational transitions of the X_1 state obtained in this work and the infrared absorption spectra of $X_2 \leftrightarrow X_1$ transitions by Ziebarth *et al.* [28].

B. Incorporation of hyperfine and field-dependent effects

We now consider a spin-rotational Hamiltonian $\mathbf{H}_{\mathrm{SR}}$ that incorporates not only rotational interaction $\mathbf{H}_{\mathrm{rot}}$ leading to the rotational energies $U_-(J,p_s)$, but also the interaction of the nuclear spins with electronic spin, with molecular rotation, and with each other. In addition, we consider the effect of external magnetic and electric fields. To incorporate all of these effects we employ the following spin-rotational Hamiltonian:

$$\mathbf{H}_{\mathrm{SR}} = \mathbf{H}_{\mathrm{rot}} + \mathbf{H}_0 + \mathbf{H}_1 + \mathbf{H}_{\mathrm{ext}}. \quad (2)$$

The interaction $\mathbf{H}_{\mathrm{rot}}$ describes the spin-rotational motion of the molecule, neglecting all nuclear spin. The interaction $\mathbf{H}_0$ describes the hyperfine structure that results from the Frosch and Foley picture [29] of the interaction of nuclear spin with an electron in a specified quantum orbit. The interaction $\mathbf{H}_1$ gives small corrections to the hyperfine structure that involve nuclear-spin-rotational and nuclear-spin-spin (bipolar) interactions. Finally, $\mathbf{H}_{\mathrm{ext}}$ describes the interaction of the molecule with external fields. For the lowest rotational states studied here, $\mathbf{H}_{\mathrm{rot}}$ is an interaction that is typically of the order of 5–50 GHz, $\mathbf{H}_0$ is an interaction of 0.2–10 GHz, and the interaction strength of $\mathbf{H}_1$ is of the order of 10–100 kHz. The microwave data are taken in fields comparable to the Earth's field, which creates Zeeman interactions on the order of 10 kHz. The optical spectroscopy takes place in an electric field on the order of 1 kV/cm which creates Stark interactions on the order of 0.1 GHz.

For the ground $^2\Pi_{1/2}$ state of the molecule, we have

$$\mathbf{H}_{\mathrm{rot}} = U_-(J,p_s), \quad (3)$$
$$\mathbf{H}_0 = \mathbf{I}_1' \cdot \widehat{A}_1 \cdot \mathbf{S}' + \mathbf{I}_2' \cdot \widehat{A}_2 \cdot \mathbf{S}', \quad (4)$$
$$\mathbf{H}_1 = (c_1\,\mathbf{I}_1\cdot\mathbf{J} + c_2\,\mathbf{I}_2\cdot\mathbf{J}) - t_0[3\,(\mathbf{I}_1'\cdot\mathbf{n}')(\mathbf{I}_2'\cdot\mathbf{n}') - (\mathbf{I}_1\cdot\mathbf{I}_2)] + (d_{c_1}\,\mathbf{I}_1\cdot\mathbf{J} + d_{c_2}\,\mathbf{I}_2\cdot\mathbf{J})\,(\mathbf{J}'\cdot\mathbf{S}'), \quad (5)$$
$$\mathbf{H}_{\mathrm{ext}} = \mu_B\mathbf{B}'\cdot\widehat{G}\cdot\mathbf{S}' + d\,\mathbf{E}'\cdot\mathbf{n}' - g_1\,\mu_N\mathbf{B}\cdot\mathbf{I}_1 - g_2\,\mu_N\mathbf{B}\cdot\mathbf{I}_2. \quad (6)$$

TABLE I. Hund's case (a) parameters used to obtain a global fit to the $^2\Pi_{3/2} \rightarrow {}^2\Pi_{1/2}$ spectra of Ref. [28] and the pure rotational spectra of this work. For $^{204}Pb^{19}F$, $^{206}Pb^{19}F$, and $^{208}Pb^{19}F$, the first value listed is from this work. For $^{207}Pb^{19}F$, the first value is work derived from our experiment but was presented in another publication [16]. Numbers in parentheses give the error in the least-significant digit. Errors are 1σ. Underlined digits do represent significant constraints on the parameters; however, because of correlations between parameters, these extra underlined digits of precision are required in order to reproduce our modeled transition frequencies to 0.1 kHz. Fixed parameters are not determined from the fit, but rather by interpolation of parameters for the other isotopes.

	$^{204}Pb^{19}F$	$^{206}Pb^{19}F$	$^{207}Pb^{19}F$	$^{208}Pb^{19}F$
A (MHz)	248 117 698(fixed)	–	248 117 014 (2)	248 116 740 (2)
	–	248 117 208(3)[a]	248 117 020 (6)[a]	248 116 740 (3)[a]
$\widetilde{A}_H$ (MHz)	0.000 090(fixed)	–	–	0.000 0897(6)
	–	0.000 090(1)[a]	0.000 089 9(3)[a]	0.000 090(1)[a]
$\widetilde{A}_D$ (MHz)	157.8964(3)	–	157.66$\underline{7}$(30)	157.595$\underline{2}$(40)
	–	157.723$\underline{8}$(30)[a]	157.66(2)[a]	157.595(6)[a]
B (MHz)	69 264.705(fixed)	6920.7279(7)	6917.910$\underline{8}$(10)	6915.114$\underline{8}$(20)
	–	6920.59(6)[a]	6917.7(1)[a]	6915.115(2)[a]
D (MHz)	0.005 44(fixed)	–	0.005 53(2)	0.005 476(7)
	–	0.005 45(2)[a]	0.005 46(6)[a]	0.005 47(2)[a]
p (MHz)	−4150.380$\underline{5}$(20)	−4146.9311(8)	−4145.2304(3)	−4143.549 0$\underline{7}$(30)
	–	−4146.1(3)[a]	−4150.0(6)[a]	−4143.1(3)[a]
p_D (MHz)	−0.002 7$\underline{7}$(30)	−0.003 2$\underline{8}$(10)	−0.0031(4)	−0.003 14(3)
	–	−0.0036(1)[b]	−0.009(2)	−0.0033(1)[b]

[a]From Ref. [28].
[b]This value is taken to be a factor of 10 greater than that reported in Ref. [28]. A reanalysis of these data suggests that the reported value of p_D is off because of a typographical error.

Here and elsewhere in this paper, the subscripts 1 and 2 refer to nuclear constants of fluorine and lead, respectively. Primes indicate quantities in the body-fixed frame of the molecule whereas quantitites without primes are taken with respect to the laboratory frame. (Primes are added to frame-independent dot products and contraction of tensors in order to give an indication of how matrix elements are determined.) The vector $\mathbf{n}'$ gives the direction of the internuclear axis. The angular-momentum operators $\mathbf{I}_1$, $\mathbf{I}_2$, and $\mathbf{J}$ act on the angular momentum of the fluorine and lead nuclei and on the total

TABLE II. Hyperfine constants. The number in parentheses gives the error of the least-significant digit. Errors from this work are 1σ. Fixed parameters are not determined from the fit, but rather by interpolation of parameters for the other isotopes. For $Pb^{19}F$ and $^{208}Pb^{19}F$, the first value listed is from this work. For $^{207}Pb^{19}F$, the first value is work derived from our experiment but was presented in another publication [16].

	$^{204}Pb^{19}F$	$^{206}Pb^{19}F$	$^{207}Pb^{19}F$	$^{208}Pb^{19}F$
$A_{\|1}$ (MHz)	409.906 (fixed)	409.906(1)	409.906 (fixed)	409.906(1)
				392 ± 64[c]
$A_{\perp 1}$ (MHz)	255.9924 (fixed)	255.9916(6)	255.991 (fixed)	255.9909(7)
				254 ± 11[c]
c_1 (MHz)	0.0093 (fixed)	0.0093(3)	0.0093 (fixed)	0.0093(2)
d_{c_1} (MHz)	0.000 56 (fixed)	0.000 56 (fixed)	0.000 56 (fixed)	0.000 5$\underline{6}$(10)
			10 146.6733(9)	
$A_{\|2}$ (MHz)			10 300 ± 800[a]	
			9727[d]	
$A_{\perp 2}$ (MHz)			−7264.0388(4)	
			7200 ± 150[a]	
			7243 ± 12[b]	
			−6860[d]	
c_2 (MHz)			0.0368(1)	
d_{c_2} (MHz)			−0.007(2)	
t_0 (MHz)			0.0022(6)	

[a]From Ref. [13]. The discrepancy in the sign of $A_{\perp 2}$ is due to a mistake in the expression for the energy levels. The observed energy-level structure is consistent with this work.
[b]From Ref. [28]. This work reports the Frosch and Foley parameter $d = -A_{\perp 2}$. Neither the sign of this term nor the predicted level structure of this work is in agreement with the present data.
[c]From Ref. [25].
[d]*Ab initio* calculation of Ref. [33].

angular momentum of the molecule neglecting nuclear spin, respectively. The pseudo-angular-momentum operator $\mathbf{S}'$ acts on the projection of angular momentum Ω on the body-fixed axis. The tensor contractions $\mathbf{I}' \cdot \widehat{A} \cdot \mathbf{S}'$ and $\mathbf{B}' \cdot \widehat{G} \cdot \mathbf{S}'$ can be written in terms of spherical tensor contractions in the following manner:

$$\mathbf{I}' \cdot \widehat{A} \cdot \mathbf{S}' = A_{||}\mathbf{I}_0^{1\prime}\mathbf{S}_0^{1\prime} - A_{\perp}\left(\mathbf{I}_1^{1\prime}\mathbf{S}_{-1}^{1\prime} + \mathbf{I}_{-1}^{1\prime}\mathbf{S}_1^{1\prime}\right), \quad (7)$$

$$\mathbf{B}' \cdot \widehat{G} \cdot \mathbf{S}' = G_{||}\mathbf{B}_0^{1\prime}\mathbf{S}_0^{1\prime} - G_{\perp}\left(\mathbf{B}_1^{1\prime}\mathbf{S}_{-1}^{1\prime} + \mathbf{B}_{-1}^{1\prime}\mathbf{S}_1^{1\prime}\right). \quad (8)$$

For the case of ^{207}Pb^{19}F, nine nuclear interaction parameters are used to describe our spectra. Four of these parameters ($A_{||1}$,$A_{\perp 1}$, $A_{||2}$, and $A_{\perp 2}$) are determined by weighted combinations of Frosch and Foley parameters a, b, c, and d, as described in the Appendix and elsewhere [15]. Two of these parameters (c_1 and c_2) describe the interaction of the nuclear magnetic moments with the magnetic field of nuclear rotation (see Ref. [30], p. 535.) The spectra are also sensitive to the parameter t_o describing the nuclear bipolar (magnetic dipole-dipole) interaction (see Ref. [30], p. 558.) Finally, the observed ^{207}Pb^{19}F spectra could not be fitted without the introduction of an additional interaction parametrized by d_{c_1} and d_{c_2} and described in the next paragraphs. For the case of $^{(\text{even})}$Pb^{19}F molecules, the four nuclear interaction parameters $A_{||1}$, $A_{\perp 1}$, c_1, and d_{c_1} are used to describe the spectra. The field-dependent interactions are described by three parameters $G_{||}$,$G_{\perp}$, and d. Here $G_{||}$ and $G_{\perp}$ are body-fixed g factors and d is the dipole moment of the molecule. The nuclear g factors g_1 and g_2 are fixed to published atomic values [31]. The dependence of $G_{||}$ and $G_{\perp}$ on the nature of the electronic wave function is given in the Appendix.

The nuclear bipolar interaction supports the physical validity of the the higher-order hyperfine correction matrix $\mathbf{H}_1$. The nuclear bipolar interaction parameter t_0 is given by the mean value of $g_1 g_2 \mu_N^2/(4\pi R^3)$ where R gives the bond distance. As such, t_0 can be used to determine a bond length $R_t = \langle R^{-3}\rangle^{-1/3} = 2.2$ Å. This is in reasonable agreement with the bond length determined from the rotational constant $R_B = \langle R^{-2}\rangle^{-1/2} = 2.05$ Å. The two additional parameters d_{c_1} and d_{c_2} do not appear in the previous literature and hence warrant some discussion. The guidance of either theory or more precise experiment would be required to pin down the precise origin of this interaction. Here we give two possibilities. The interaction that appears in Eq. (5) may describe an Ω-doubling-state dependence to the nuclear-spin-nuclear-rotational coupling. Such an interaction would be caused by the relativistic transformation of the electronic electric field to a magnetic field in the frame of the moving nuclei. It is reasonable to assume that this relativistic magnetic field will depend on the Ω-doubling state and necessitate the corrections d_{c_1} and d_{c_2} to the more usual nuclear-spin-nuclear-rotation coupling constants c_1 and c_2. A second interpretation is a centrifugal correction to the hyperfine interaction. In the Appendix we show that for a $^2\Pi_{1/2}$ state, the hyperfine parameters $A_{\perp 1}$ and $A_{\perp 2}$ are related to the Frosch and Foley parameters by $A_{\perp 1} = -d_1$ and $A_{\perp 2} = -d_2$. The parameter d_{c_2} can be interpreted as a centrifugal correction to the Frosch and Foley d_2 parameter for the lead nucleus with $A_{\perp 2} \approx -d_2 + d_{c_2} J(J+1)$. Specifically, the spectroscopic correction d_{c_2} may come from the interaction

$$\mathbf{H}_{d_2} = \frac{d_{c_2}}{2}\left[\mathbf{J}^2\left(\mathbf{I}_1^{1\prime}\mathbf{S}_{-1}^{1\prime} + \mathbf{I}_{-1}^{1\prime}\mathbf{S}_1^{1\prime}\right) + \left(\mathbf{I}_1^{1\prime}\mathbf{S}_{-1}^{1\prime} + \mathbf{I}_{-1}^{1\prime}\mathbf{S}_1^{1\prime}\right)\mathbf{J}^2\right]. \quad (9)$$

TABLE III. Observed pure rotational transition frequencies ν_{obs} of the X_1 state of even isotopes of PbF in units of MHz. The values in parentheses give the 1σ experimental error of the last digit of precision. The deviation of our fit from observation is given by $\Delta = \nu_{\text{fit}} - \nu_{\text{obs}}$ in units of the last digit of precision (100 Hz).

	^{204}Pb^{19}F		^{206}Pb^{19}F		^{208}Pb^{19}F	
Levels	ν_{obs} (MHz)	Δ	ν_{obs} (MHz)	Δ	ν_{obs} (MHz)	Δ
1–3			3925.8973(15)[a]	−100	3922.5065(20)	−6
2–4			4198.1599(15)	−7	4194.7773(7)	−1
1–4			4233.0993(7)	17	4229.7176(30)	15
6–7			8124.0646(10)	5	8117.3017(10)	−8
5–7			8206.6112(30)	10	8199.8478(9)	4
6–8			8314.2844(7)	−12	8307.5180(20)	−2
5–8	8403.7241(6)	−1	8396.8302(10)	2	8390.0664(20)	−12
10–11			–		12 277.6822(7)	1
4–7			–		12 374.6701(7)	0
4–8			–		12 443.8577(7)	6
9–12			–		12 540.8465(8)	−5
14–15			–		16 428.5160(10)	2
13–16			–		16 688.4929(20)	17
1–5	18 444.7873(5)	2	18 429.5427(5)	−2	18 414.5880(5)	1
2–6	18 492.3922(5)	8	18 477.1479(5)	1	18 462.1933(5)	2
1–6	18 527.3355(5)	−8	18 512.0902(5)	−5	18 497.1352(5)	2
4–7	22 421.7437(6)	−2	22 403.0538(5)	0	22 384.7171(5)	1
4–8	22 611.9629(6)	−2	22 593.2718(5)	1	22 574.9344(5)	−2
3–7	22 728.9569(6)	6	22 710.2674(5)	1	22 691.9306(5)	−2

[a]Value not consistent with combination differences of other transitions, and hence not used in our fit.

If one ignores terms that are off diagonal in J, this interaction is identical to the interaction proportional to d_{c_2} that appears in Eq. (5).

The Appendix gives matrix elements of $\mathbf{H}_{\mathrm{SR}}$ in a basis of total angular momentum F and M, spin-rotational angular momentum J, total nuclear angular momentum I, and electronic parity $p_s = \pm 1$. Specifically, the basis is given by

$$|F,I,J,M,p_s\rangle = \sum_{M_J,M_I} \langle I,M_I,J,M_J|F,M\rangle |J,M_J,p_s\rangle |I,M_I\rangle. \quad (10)$$

An omega ($\Omega = \pm\frac{1}{2}$) basis set is related to this parity ($p_s = \pm 1$) basis set by

$$|F,I,J,M,p_s\rangle = \frac{1}{\sqrt{2}}\left(\left|F,I,J,M,\Omega=\frac{1}{2}\right\rangle + p_s(-1)^{J-1/2}\left|F,I,J,M,\Omega=\frac{-1}{2}\right\rangle\right). \quad (11)$$

We note that Eq. (11) is consistent with Kopp and Hougen [32] as well as Brown and Carrington [30], but is in disagreement with Kozlov *et al.* [9] which carries an error in the sign of the coefficient of the $\Omega = -1/2$ wave function. This minor error has led to discrepancies between theory and experiment in the literature and prevented the prediction of states in ^{207}Pb^{19}F with exaggerated polarizability [13]. This issue is discussed further in Sec. IV and in the companion article to this one [33].

IV. ANALYSIS OF HYPERFINE AND ROTATIONAL CONSTANTS

In the absence of external fields, the energy levels of $^{(\mathrm{even})}$Pb^{19}F molecules are found by diagonalization of the sum of the 2×2 hyperfine interaction matrix of Table VII and the diagonal spin-rotational energy $U_-(J,p_s)$. Similarly, the energy-level structure of ^{207}Pb^{19}F is found by diagonalization of the sum of the 4×4 hyperfine interaction matrices of Tables VIII and IX and the diagonal spin-rotational energy. The energy levels found in this way are cross-checked between independently written codes (one by N.E.S.-R., the other by T.J.S.) In addition, computed energy levels ignoring the high-order corrections of H_1, but including the external electric and magnetic fields, were checked against the independently written codes of Kozlov and Petrov of the Saint Petersburg Nuclear Physics Institute in Russia. We note that only one of these four codes makes use of the *F-M-I-J-*p_s basis presented here.

We have carried out a global fit to the field-free spectra of the $X_2 \leftrightarrow X_1$ transition [28] and the pure rotational microwave spectra of the X_1 state reported in this work. These values are reported in Tables I and II. Some of the values appearing in these tables are given to more significant figures than are determined by our fit. Inclusion of these extra digits is required to reproduce the line positions to 0.1 kHz. This requirement is a result of correlations between fitted parameters. The observed microwave transitions, along with deviations of our fit from these values, are given in Tables III and IV.

For ^{206}Pb^{19}F we are able to determine improved values for the rotational constant B and the Ω-doubling constants p and p_D. We also report for the first time values of the hyperfine parameters for fluorine: $A_{||1}$, $A_{\perp 1}$, and c_1. The data set for the ^{208}Pb^{19}F molecule covers a greater range of rotational levels. As a result, we are able to determine improved values for A, B, $\widetilde{A}_D$, D, p, p_D, and the hyperfine parameters for fluorine: $A_{\perp 1}$ and $A_{||1}$. We are also able to report for the first time a value of the fluorine nuclear-spin-rotational interaction c_1 and the nuclear-rotational correction parameter d_{c1}. With the exception of p_D, our newly measured parameters for ^{206}Pb^{19}F and ^{208}Pb^{19}F are in agreement with previous results [15,28]. A reanalysis of the data presented by Ziebarth and coworkers [28] suggests that a typographical error led to a factor of 10 error in the reported value of p_D.

For the less abundant ^{204}Pb^{19}F molecule, Ziebarth and coworkers did not publish any high-resolution spectroscopy. In addition, we observed only seven microwave transitions. To analyze this limited data set, we fitted the microwave spectra to find p, p_D, and $\widetilde{A}_D$. For this case, the rotational constant B was extrapolated by linear interpolation of the other isotopes

TABLE IV. Observed pure rotational transition frequencies ν_{obs} of the X_1 state of ^{207}Pb^{19}F in units of MHz. The values in parentheses give the 1σ experimental error of the last digit of precision. The deviation of our fit from observation is given by $\Delta = \nu_{\mathrm{fit}} - \nu_{\mathrm{obs}}$ in units of the last digit of precision (100 Hz).

	^{207}Pb^{19}F	
Levels	ν_{obs}(MHz)	Δ
3–6	3187.4875(20)	5
2–6	3219.8137(7)	−3
10–11	4455.4540(25)	21
9–12	4699.2265(25)	29
1–4	8495.0022(7)	1
18–19	8620.5475(10)	−8
1–5	8687.2098(7)	6
8–13	11 682.5211(7)	6
7–13	11 715.3703(7)	−14
8–14	11 867.6415(10)	−8
7–14	11 900.4870(7)	9
3–7	14 430.1830(5)	13
2–7	14 462.5104(5)	−8
3–8	14 463.0311(5)	3
2–8	14 495.3580(5)	−11
16–21	15 865.1888(5)	−8
15–22	16 108.7271(5)	−4
2–9	18 333.5013(5)	3
3–10	18 380.8711(5)	5
2–10	18 413.1982(5)	−12
5–11	22 377.8342(5)	2
5–12	22 541.9123(5)	−1
4–11	22 570.0427(5)	−2
1–7	22 658.9018(5)	−5
1–8	22 691.7486(5)	−2
6–13	22 958.0652(5)	−1
6–14	23 143.1846(5)	−4
5–13	25 687.0601(5)	−4
5–14	25 872.1789(5)	−1
4–13	25 879.2667(5)	12
4–14	26 064.3873(5)	−3

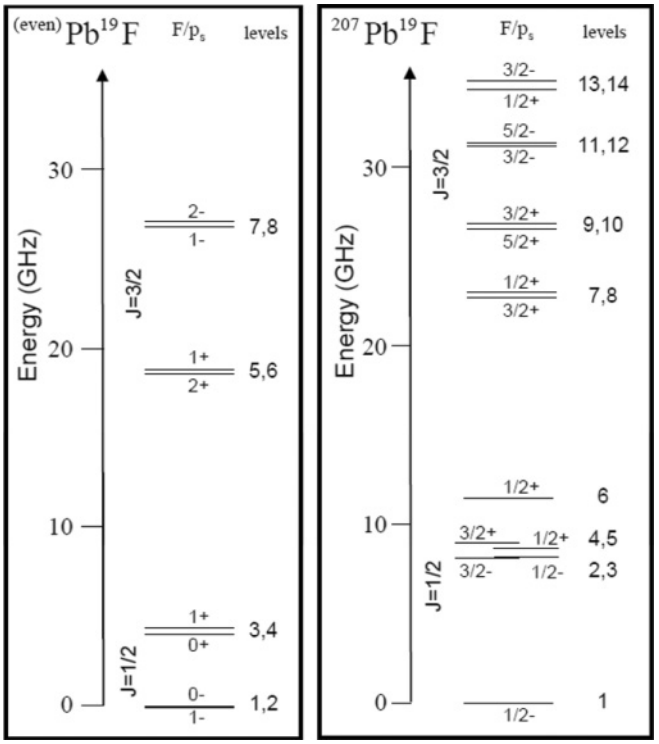

FIG. 1. Hyperfine energy-level structure of the lowest lying states of $X_1(v = 0)$ of $^{(even)}Pb^{19}F$ (left-hand side) and $^{207}Pb^{19}F$ (right-hand side).

with respect to inverse reduced mass. All other spectroscopic parameters were extrapolated from the other isotopes by linear interpolation with respect to reduced mass.

In a preliminary analysis of the microwave structure of $^{207}Pb^{19}F$, the parameters $A_{||1}$, $A_{\perp 1}$, c_1, and d_{c1} were not significantly different from the average value of the fitted $^{206}Pb^{19}F$ and $^{208}Pb^{19}F$ parameters. For this reason, these values were fixed to this average in our final analysis. We were then able determine improved values for A, B, $\widetilde{A}_D$, D, p, p_D, $A_{\perp 2}$ and $A_{||2}$ and report, for the first time a value for the lead nuclear-spin-rotational interaction parameter c_2, the nuclear-rotation correction parameter d_{c2}, and the nuclear bipolar interaction parameter t_0. We note that for $^{207}Pb^{19}F$, our measured values of p and p_D are very close to what one might expect from mass scaling the $^{(even)}Pb^{19}F$ values, but are not in agreement with the values reported by Ziebarth and coworkers [28]. A reanalysis of their data suggests that the value of p for the $^{204}Pb^{19}F$ molecule might have inadvertently been placed in the table of $^{207}Pb^{19}F$ parameters.

The only nontrivial disagreement with previous results is in the hyperfine parameter $A_{\perp 2}$. Whereas the magnitude of our reported value of $A_{\perp 2}$ is in agreement with two previous reported values, the sign is not. We believe both of these previous works to be in error. For the case of the work of Ziebarth *et al.* [28], sensitivity to $A_{\perp 2} = -d$ was gained primarily through high-lying states for which the sign of the splitting is difficult to ascertain. Ziebarth and coworkers present an inferred energy level diagram of the $J = 1/2$ state

TABLE V. Energy-level structure (in MHz) of the first 22 states of the PbF molecule as determined from the parameters appearing in Tables I and II. Here $F_2 = J + I_2$ where I_2 gives the nuclear spin of ^{207}Pb.

Level	J	p_s	F	$^{204}Pb^{19}F$	$^{206}Pb^{19}F$	$^{208}Pb^{19}F$	Level	J	p_s	F_2	F	$^{207}Pb^{19}F$ (MHz)
22	$\frac{11}{2}$	+	5	229 342.451	229 153.049	228 967.283	22	$\frac{5}{2}$	+	2	$\frac{5}{2}$	709 19.300
21	$\frac{11}{2}$	+	6	229 230.539	229 041.137	228 855.371	21	$\frac{5}{2}$	+	2	$\frac{3}{2}$	70 755.337
20	$\frac{9}{2}$	+	5	176 860.293	176 714.230	176 570.892	20	$\frac{5}{2}$	+	3	$\frac{7}{2}$	67 474.609
19	$\frac{9}{2}$	+	4	176 710.617	176 564.555	176 421 217	19	$\frac{5}{2}$	+	3	$\frac{5}{2}$	67 320.236
18	$\frac{9}{2}$	−	4	156 100.274	155 971.391	155 844.981	18	$\frac{5}{2}$	−	3	$\frac{5}{2}$	58 699.689
17	$\frac{9}{2}$	−	5	155 991.412	155 862.531	155 736.120	17	$\frac{5}{2}$	−	3	$\frac{7}{2}$	58 604 206
16	$\frac{7}{2}$	−	4	113 162.011	113 068.56	112 976.87	16	$\frac{5}{2}$	−	2	$\frac{3}{2}$	54 890.149
15	$\frac{7}{2}$	−	3	113 006.385	112 912.94	112 821.24	15	$\frac{5}{2}$	−	2	$\frac{5}{2}$	54 810.573
14	$\frac{7}{2}$	+	3	96 550.596	96 470.886	96 392.727	14	$\frac{3}{2}$	−	1	$\frac{3}{2}$	34 559.389
13	$\frac{7}{2}$	+	4	96 446.215	96 366.532	96 288.367	13	$\frac{3}{2}$	−	1	$\frac{1}{2}$	34 374.270
12	$\frac{5}{2}$	+	3	63 157.755	63 105.616	63 054.459	12	$\frac{3}{2}$	−	2	$\frac{5}{2}$	31 229.123
11	$\frac{5}{2}$	+	2	62 991.577	62 939.440	62 888.283	11	$\frac{3}{2}$	−	2	$\frac{3}{2}$	31 065.045
10	$\frac{5}{2}$	−	2	50 693.414	50 651.608	50 610.601	10	$\frac{3}{2}$	+	2	$\frac{3}{2}$	22 609.589
9	$\frac{5}{2}$	−	3	50 596.426	50 554.620	50 513.613	9	$\frac{3}{2}$	+	2	$\frac{5}{2}$	26 529.893
8	$\frac{3}{2}$	−	2	26 848.512	26 826.373	26 804.653	8	$\frac{3}{2}$	+	1	$\frac{1}{2}$	22 691.749
7	$\frac{3}{2}$	−	1	26 658.293	26 636.155	26 614.436	7	$\frac{3}{2}$	+	1	$\frac{3}{2}$	22 658.901
6	$\frac{3}{2}$	+	1	18 527.335	18 512.090	18 497.135	6	$\frac{1}{2}$	+	0	$\frac{1}{2}$	11 416.205
5	$\frac{3}{2}$	+	2	18 444.788	18 429.543	18 414.588	5	$\frac{1}{2}$	+	1	$\frac{3}{2}$	8687.210
4	$\frac{1}{2}$	+	1	4236.549	4233.101	4229.719	4	$\frac{1}{2}$	+	1	$\frac{1}{2}$	8495.002
3	$\frac{1}{2}$	+	0	3929.335	3925.887	3922.506	3	$\frac{1}{2}$	−	1	$\frac{1}{2}$	8228.717
2	$\frac{1}{2}$	−	0	34.942	34.942	34.942	2	$\frac{1}{2}$	−	1	$\frac{3}{2}$	8196.392
1	$\frac{1}{2}$	−	1	0	0	0	1	$\frac{1}{2}$	−	0	$\frac{1}{2}$	0

that is in marked disagreement with our direct observation. For the work of McRaven *et al.* [12], the $A \leftarrow X_1$ transition was observed for several low-J rotational levels. This observation allowed the determination of a hyperfine energy-level structure that is in agreement with what we observe here. However, a phase error in the parity wave functions led to a sign error in the spin-rotational energy which in turn led to a sign error in the reported value of $A_{\perp 2}$. This minor error can be traced back to the work of Kozlov *et al.* [9].

The energy-level structure of the PbF molecule as determined from our fit is given in Fig. 1 and Table V. The hyperfine structure of ^{207}Pb^{19}F has an important consequence for an *e*EDM experiment that was first suggested in the 2008 observation of McRaven *et al.* [13]: the closely spaced states of opposite parity in the $J = 1/2$ manifold cause ^{207}Pb^{19}F to have ten times the polarizability of ^{204}Pb^{19}F, ^{206}Pb^{19}F, and ^{208}Pb^{19}F. This implies *e*EDM experiments utilizing ^{207}Pb^{19}F can be carried out at an electric field well below 1000 V/cm.

V. EVALUATION OF THE ZEEMAN PARAMETERS OF THE $X_1(v = 0)$ STATE OF ^{208}Pb^{19}F

First-order perturbation theory can be used to determine the state-dependent g factors of the PbF molecule. For $^{(even)}$Pb^{19}F, the eigenvalues and eigenvectors of the field-free Hamiltonian may be evaluated analytically and, as a consequence, analytic expressions for the g factors may be obtained. Details of this derivation are given elsewhere [34], with the result

$$g(F,J,p_s) = \frac{1}{2F+1}\left(\frac{1}{2J+1} + \frac{J-F}{\sqrt{F(F+1)}}\sin 2\theta + \frac{(J-F)}{F(F+1)}\sin^2\theta\right)G_{||} + (-1)^{J-1/2}p_s \times \left(\frac{1}{2F+1}\cos 2\theta + \frac{\sin 2\theta}{2\sqrt{F(F+1)}}\right)G_{\perp} + \left(-\frac{\mu_N}{\mu_B}\right)\left(\frac{2(F-J)}{2J+1}\cos 2\theta + \frac{1}{2F(F+1)}\sin^2\theta\right)g_1, \quad (12)$$

where

$$\theta = \frac{1}{2}\arctan\left[\frac{2\sqrt{F(F+1)}[A_{||1} + (-1)^F p_s A_{\perp 1}]}{2B(2F+1)^2 - A_{||1} - (-1)^F p_s[A_{\perp 1} + (2F+1)^2 p]}\right]. \quad (13)$$

Here θ is an angle that describes the mixing between the $J = F - 1/2$ and $J = F + 1/2$ states and $A_{||1}$ and $A_{\perp 1}$ are parameters that account for the fluorine hyperfine interaction. We also have included the effect of the nuclear magnetic moment of the fluorine. (In the evaluation of the angle θ, we ignored higher-order corrections to the rotational energy.)

Details of the reduction of the fit of our observed Zeeman line splittings ΔU to the parameters $G_{\perp}$ and $G_{||}$ are given elsewhere [35] and described briefly in what follows. In order to reduce the contribution of uncertainty of the measurement to the calibration of the magnetic field, we first determine the ratio $G_{||}/G_{\perp}$. Here we use Helmholtz coils to create a magnetic field that is perpendicular to the electric field vector of the microwave radiation. We then observe the Zeeman splitting of the following two $F = 0 \leftrightarrow F = 1$ transitions:

$$\left([2], J = \tfrac{1}{2}, F = 0, p_s = -1\right) \leftrightarrow \left([6], J = \tfrac{3}{2}, F = 1, p_s = +1\right), \quad 18.462\,193\ \text{GHz}, \quad \text{(A)}$$

$$\left([3], J = \tfrac{1}{2}, F = 0, p_s = +1\right) \leftrightarrow \left([7], J = \tfrac{3}{2}, F = 1, p_s = -1\right), \quad 22.691\,931\ \text{GHz}. \quad \text{(B)}$$

The numbers in square brackets refer to the energy-level diagram of Fig. 1. The ratio $G_{||}/G_{\perp}$ is then found by taking the following field-independent ratio of Zeeman splittings:

$$\Gamma_{AB} = 4\frac{\Delta U_B + \Delta U_A}{\Delta U_B - \Delta U_A}, \quad (14)$$

$$= 4\frac{|\Delta U_B| - |\Delta U_A|}{|\Delta U_B| + |\Delta U_A|} \text{ for } |\Gamma_{AB}| < 4, \quad (15)$$

$$\approx 0.0046 + 1.009\frac{G_{||}}{G_{\perp}} + 2.991\frac{g_1}{G_{\perp}}\frac{\mu_N}{\mu_B}, \quad (16)$$

$$= -0.371 \pm 0.005\ \text{(expt.)}. \quad (17)$$

It is necessary to express Γ_{AB} in terms of absolute values of the splittings because the experiment is not sensitive to the sign of the splittings, only the magnitude. If hyperfine rotational mixing is not considered, then $\theta = 0$ and $\Gamma_{BA} = G_{||}/G_{\perp} - 3g_1\mu_N/(\mu_B G_{\perp})$. We can also make the approximation $3g_1\mu_N/(\mu_B G_{\perp}) \approx 0.026$ by assuming the CRC Handbook [31] value for $g_1 = g_F = 5.25773$ and $G_{\perp} = -0.326$ (Ref. [9]). This approximation indicates that the nuclear Zeeman effect is roughly a factor of 5 larger correction to the Zeeman interaction than the effect of hyperfine mixing of different rotational states.

Prediction of the Zeeman splittings for each state requires the value of g_1 and the body-fixed g factors $G_{||}$ and $G_{\perp}$. The value of g_1 is taken from the literature [31] whereas the value of $G_{||}$ is determined from $G_{\perp}$ and g_1 using the measured value of Γ_{AB} and the relationship of Eq. (16). Thus 16 measured Zeeman line splittings can be fitted in terms of the single parameter $G_{\perp}$. This determination of $G_{\perp}$ is limited by our magnetic field calibration. A zero magnetic field is created by adjusting currents to Helmholtz coils until all Zeeman splittings are minimized. To apply a magnetic field parallel to the microwave polarization, the current on the vertical Helmholtz coil is turned off. To apply a magnetic field perpendicular to the microwave polarization, the current on the horizontal Helmholtz coil is turned off. We assume the magnetic field can be determined from the change in current in each coil. As a test of this assumption, we make two experimental determinations of $G_{\perp}$, one by

TABLE VI. Field parameters of the $X_1(v=0)$ state of $^{208}Pb^{19}F$.

	This work (66% C.L.)	Ref. [9]	Ref. [10]	Ref. [33]
$G_\perp$	-0.38 ± 0.02	$-0.438 < G_\perp < -0.269$	-0.326	-0.319
$G_\parallel$	0.12 ± 0.01	$0.034 < G_\parallel < 0.114$	0.040	0.082
d_{X_1}	3.5 ± 0.3 D	–	4.62 D	4.26 D
d_A	2.8 ± 0.2 D			2.51 D

considering the parallel magnetic field ($\Delta M = 0$ transitions) and a second by considering the perpendicular magnetic field ($\Delta M = \pm 1$ transitions). The resulting values are

$$G_\perp = -0.39 \pm 0.01_{\text{statistical}} \text{ (expt., } \Delta M = 0 \text{ transitions)}, \tag{18}$$

$$G_\perp = -0.38 \pm 0.01_{\text{statistical}} \text{ (expt., } \Delta M = 1 \text{ transition)}. \tag{19}$$

The result of this analysis indicates that our magnetic field calibration creates an error that is roughly equal to the statistical error of our measurement. Our final result for $G_\perp$ is given and compared to published theory in Table VI. We assume throughout the analysis presented here that $G_\perp < 0$. The result is a fit with a variance in $\Delta U_{\text{Zeeman}}/\mu_B B$ of 0.0028. Even though the experiment is insensitive to the orientation of the molecules, our data are sensitive to the sign of $G_\perp$ through the contribution of the nuclear magnetic moment g_1. A fit assuming $G_\perp > 0$ has a variance of 0.0055. Thus the Zeeman data presented here support the theoretical prediction [9] that $G_\perp < 0$.

VI. EVALUATION OF THE DIPOLE MOMENT OF THE $X_1(v=0)$ STATE OF $^{208}Pb^{19}F$

The determination of the dipole moment of the $X_1(v=0)$ state of $^{208}Pb^{19}F$ was carried out at the University of Oklahoma. Specifically, the optical transition frequency of the following two $X_1(v=0) \leftrightarrow A(v=1)$ transitions are determined as a function of the electric field:

$$X_1\left(J=\tfrac{1}{2}, F=1, p=-1\right) \leftrightarrow A\left(J=\tfrac{3}{2}, F=2, p=1\right), \quad 686\,484 \text{ GHz} \quad \left(R_{ff+}\left[\tfrac{1}{2}\right]\right),$$

$$X_1\left(J=\tfrac{3}{2}, F=2, p=-1\right) \leftrightarrow A\left(J=\tfrac{1}{2}, F=1, p=1\right), \quad 686\,391 \text{ GHz} \quad \left(P_{ee+}\left[\tfrac{1}{2}\right]\right).$$

The expected shifts of these transitions as a function of electric field are the eigenvalues of the sum of the diagonal spin-rotational matrix elements $U_-(J, p_s)$, the 2×2 block-diagonal hyperfine matrix elements (Table VII), and the Stark interaction matrix elements [Eq. (A24)]. To determine the A-state contribution of the shift of each line, we use spin-rotational constants determined by Lumley and Barrow [36] and hyperfine constants determined by Sivakumar *et al.* [15].

The final result of this numerical analysis is

$$\Delta U\left(R_{ff+}\left[\tfrac{1}{2}\right]\right) = \left[0.53\left(\frac{d_A}{\text{D}}\right)^2 + 10.35\left(\frac{d_{X_1}}{\text{D}}\right)^2\right] \times \left(\frac{E}{\text{kV cm}^{-1}}\right)^2 \text{MHz}, \tag{20}$$

$$\Delta U\left(P_{ee+}\left[\tfrac{3}{2}\right]\right) = -\left[7.67\left(\frac{d_A}{\text{D}}\right)^2 + 0.95\left(\frac{d_{X_1}}{\text{D}}\right)^2\right] \times \left(\frac{E}{\text{kV cm}^{-1}}\right)^2 \text{MHz}. \tag{21}$$

The dipole moments d_A and d_{X_1} are found by fitting these frequency-dependent shifts at $E = 0.236$ kV/cm, $E = 0.393$, kV/cm and $E = 0.787$ kV/cm. The determined dipole moments d_{X_1} and d_A appear in Table VI.

We note that our reported value of $d_{A,v=1} = 2.8 \pm 0.2$ D does not agree with a previously reported preliminary estimate of 5.5 ± 0.2 D [25]. This value was labeled as "preliminary" because it relied on the theoretical value $d_{X_1} = 4.62$ D [10] for the ground state. We have repeated the analysis carried out in this previous work, instead using $d_{X_1} = 3.5 \pm 0.3$ D to obtain a value $d_{A,v=1} = 3.6 \pm 0.4$ D that is in reasonable agreement with the more careful experimental study carried out in this work.

VII. SUMMARY

We report new values of spin-rotational constants, hyperfine constants, Zeeman interaction parameters, and the dipole moment of the lead monofluoride molecule. The hyperfine constants, spin-rotational constants, and Zeeman parameters are determined by carrying out pure rotational microwave spectroscopy of the $X_1(v=0)$ ground state of PbF at the Leibniz Universität Hannover. To gain sensitivity to distortion parameters, data of Ziebarth *et al.* [28] were incorporated into our fit. Sensitivity to the dipole moment of the ground state was determined by optical Stark spectroscopy carried out at the University of Oklahoma. The field-free parameters are given in Tables I and II, whereas the field parameters of the ground state of $^{208}Pb^{19}F$ are given in Table VI. The parameters found in this work are critically important to the design and interpretation of a measurement of the eEDM using the PbF molecule.

ACKNOWLEDGMENTS

Work by T.J.S. at Brookhaven National Laboratory was performed under Contract No. DE-AC02-98CH10886 with the US Department of Energy and supported by its Division

of Chemical Sciences, Geosciences, & Biosciences. Work by N.E.S.-R. was performed with support from the National Science Foundation Grant No. NSF-0855431. J.U.-G. acknowledges funding from the Deutsche Forschungsgemeinschaft (DFG) and the Land Niedersachsen, and R.J.M., B.S.M., and A.L.B. appreciate the research support provided by the Pomona College Sontag Fellowship Program. We are indebted for the thoughtful comments and cross-checking of field-dependent energy levels by Mikhail Kozlov and Aleksandr Petrov of St. Petersburg Nuclear Physics Institute.

APPENDIX: SECULAR EQUATION FOR THE HYPERFINE AND FIELD-DEPENDENT ENERGIES OF A $^2\Pi_{1/2}$ MOLECULE

Consistent with the discussion of the previous section, we let the rotational energy be given by

$$\langle F,I,J,M,p|\mathbf{H}_{\rm rot}|F,I,J,M,p_s\rangle = \delta_{FF'}\delta_{II'}\delta_{JJ'}\delta_{MM'}\delta_{p_s p'_s}\ U_-(J,p_s), \tag{A1}$$

where $U_-(J,p_s)$ is given by the lower eigenvalue of Eq. (1). In the following sections we consider the matrix elements of each of the other terms appearing in Eq. (2).

1. Hyperfine interaction and relationship of the parameters $A_{||}$ and $A_\perp$ to the Frosch and Foley parameters a, b, c, and d

The hyperfine interaction between the nuclear and electronic magnetic moments is often described in terms of the Frosch and Foley parameters a,b,c, and d [29]. In the Frosch and Foley picture, the interaction of the net electron spin and orbital angular momenta with the nuclear spin is given by [29]

$$\mathbf{H}_0 = \sum_t (-1)^t \mathbf{I}'^1_t \mathbf{Q}'^1_{-t}, \tag{A2}$$

$$\mathbf{Q}'^1_t = a\mathbf{L}'^1_t + (b+c)\mathbf{S}'^1_0\delta_{t,0} + \left(b\mathbf{S}'^1_t - de^{2it\phi}\mathbf{S}'^1_{-t}\right)\delta_{|t|,1}. \tag{A3}$$

Here $\mathbf{L}'^1_t$ and $\mathbf{S}'^1_t$ are the spherical tensor operators giving the body-fixed orbital and spin angular momentum of the molecule. For a rotating $\Omega = 1/2$ molecule that is far removed in energy from a mixed $\Omega = 3/2$ state, the hyperfine interaction with a given nucleus depends only on two expectation values:

$$A_{||} = 2\left\langle \tfrac{1}{2}\middle|\mathbf{Q}'^1_0\middle|\tfrac{1}{2}\right\rangle = -2\left\langle -\tfrac{1}{2}\middle|\mathbf{Q}'^1_0\middle|-\tfrac{1}{2}\right\rangle, \tag{A4}$$

and

$$A_\perp = \sqrt{2}\left\langle -\tfrac{1}{2}\middle|\mathbf{Q}'^1_{-1}\middle|\tfrac{1}{2}\right\rangle = -\sqrt{2}\left\langle \tfrac{1}{2}\middle|\mathbf{Q}'^1_{-1}\middle|-\tfrac{1}{2}\right\rangle. \tag{A5}$$

Here $A_{||}$ and $A_\perp$ are the parallel and perpendicular hyperfine constants. They are defined in such a way that the interaction operator $\mathbf{Q}'^1_t$ can be written as $A_t\mathbf{S}'^1_t$ where $\mathbf{S}'^1_t$ is the body-fixed spherical tensor operator for the electronic pseudo spin angular momentum with $A_0 = A_{||}$ and $A_{\pm1} = A_\perp$. If we assume that the unpaired electron has an orbital

$$\left|\frac{1}{2}\right\rangle = \sum_{\ell=0}^{\infty}\left[c^0_\ell|\ell,0\rangle\left|\frac{1}{2}\right\rangle + c^1_\ell|\ell,1\rangle\left|-\frac{1}{2}\right\rangle\right], \tag{A6}$$

then the hyperfine constants $^1A_{||}$ and $^1A_\perp$ are related to the Frosch and Foley parameters by [15]

$$A_{||} = \begin{cases} \sum_{\ell=0}^{\infty}\left\{\left|c^0_\ell\right|^2(b+c) + \left|c^1_\ell\right|^2[2a-(b+c)]\right\} & \\ b+c & \text{for a } \sigma \text{ orbital} \\ 2a-b-c & \text{for a } \pi \text{ orbital,} \end{cases} \tag{A7}$$

and

$$A_\perp = \begin{cases} \sum_{\ell=0}^{\infty}\left[a\sqrt{\ell(\ell+1)}\left(c^{1*}_\ell c^0_\ell + c^{0*}_\ell c^1_\ell\right) + b\left|c^0_\ell\right|^2 - d\left|c^1_\ell\right|^2\right] & \\ b & \text{for a } \sigma \text{ orbital} \\ -d & \text{for a } \pi \text{ orbital.} \end{cases} \tag{A8}$$

2. Secular equation of the field-free spin rotational Hamiltonian

The angular momentum algebra required to evaluate the matrix elements of Eq. (2) is given in several places [30,37]. Here we have used these techniques to find analytical expressions for each element. The molecules $^{(\rm even)}$Pb^{19}F belong to the case $I_1 = \frac{1}{2}$ and $I_2 = 0$. For this case there exists just two states that share values of F,M, and p_s. Thus the field-free energy levels may be found by diagonalizing a 2×2 matrix for which the hyperfine contribution is given in Table VII. The diagonal rotational contribution $U_-(J,p_s)$ is found by diagonalizing the matrix of Table II of Amiot *et al.* [27] or, equivalently, Eq. (1). The ^{207}Pb^{19}F molecule belongs to the case that $I_1 = I_2 = 1/2$. For this case the energy levels are found by diagonalizing a 4×4 matrix corresponding to the matrix elements for states with $(I=0,\ F=J)$,$(I=1,\ F=J)$, $(I=1,\ F=J-1)$, and $(I=1,\ F=J+1)$. Explicit forms of these matrix elements are given in Tables VIII and IX.

TABLE VII. Matrix elements of the hyperfine interaction for the case $I_1 = I = \frac{1}{2}, I_2 = 0$.

	$\langle FJ'IMp_s\|\mathbf{H}_0+\mathbf{H}_1\|FJIMp_s\rangle =$	
	$J = F+\frac{1}{2}$	$J = F-\frac{1}{2}$
$J' = F+\frac{1}{2}$	$-\frac{\chi A_{\perp1}}{4} - \frac{A_{\chi1}}{4(2F+1)} - \frac{2F+3}{4}c_{\chi1}$	$A_{\chi1}\frac{\sqrt{F(F+1)}}{2(2F+1)}$
$J' = F-\frac{1}{2}$	$A_{\chi1}\frac{\sqrt{F(F+1)}}{2(2F+1)}$	$-\frac{\chi A_{\perp1}}{4} + \frac{A_{\chi1}}{4(2F+1)} + \frac{2F-1}{4}c_{\chi1}$
$\chi = (-1)^F p_s,$	$A_{\chi1} = A_{||1} + \chi A_{\perp1},$	$c_{\chi1} = c_1 + p_s(-1)^{J-1/2}(J+\frac{1}{2})d_{c1}/2$

TABLE VIII. Matrix elements of the hyperfine interaction $\mathbf{H}_0$ for the case $I_1 = I_2 = \frac{1}{2}$. Conjugate matrix elements given trivially by the Hermitian property of $\mathbf{H}_0$ are not shown.

$\langle F J' I' M p_s \vert \mathbf{H}_0 \vert F J I M p_s \rangle$			
$I = 0$ $J = F$	$I = 1$ $J = F$	$I = 1$ $J = F + 1$	$I = 1$ $J = F - 1$
0	$-\frac{2F\chi\underline{A}_\perp + \underline{A}_\chi}{4\sqrt{F(F+1)}}$ $-\frac{2F\chi\overline{A}_\perp + \overline{A}_\chi}{4F(F+1)}$	$\sqrt{\frac{2F+3}{F+1}}\frac{2\chi\underline{A}_\perp - \underline{A}_\chi}{4}$ $\frac{-2\chi\overline{A}_\perp + \overline{A}_\chi}{4}\sqrt{\frac{(2F+3)F}{(F+1)^2}}$ $\frac{2(F+2)\chi\overline{A}_\perp - \overline{A}_\chi}{4(F+1)}$	$\frac{\underline{A}_\chi}{4}\sqrt{\frac{2F-1}{F}}$ $\frac{\overline{A}_\chi}{4}\sqrt{\frac{(F+1)(2F-1)}{F^2}}$ 0 $\frac{-2F\chi\overline{A}_\perp + \overline{A}_\chi}{4F}$
$\overline{A}_\vert = (A_{\vert 1} + A_{\vert 2})/2, \underline{A}_\vert = (A_{\vert 1} - A_{\vert 2})/2$ $\overline{A}_\perp = (A_{\perp 1} + A_{\perp 2})/2, \underline{A}_\perp = (A_{\perp 1} - A_{\perp 2})/2$ $\chi = (-1)^{F-\frac{1}{2}} p_s, \underline{A}_\chi = \underline{A}_\vert + \chi\underline{A}_\perp, \overline{A}_\chi = \overline{A}_\vert + \chi\overline{A}_\perp$			

3. Zeeman interaction

In the molecular fixed frame, the Zeeman interaction is given by

$$(\mu_B)(g\vec{S}' + \vec{L}') \cdot \vec{B}' = \mu_B \sum_t (-1)^t G'^1_{-t} B'^1_t, \tag{A9}$$

with

$$G'^1_t = \left(g S'^{1\prime}_t + L'^{1\prime}_t\right). \tag{A10}$$

We relate the tensor G'^1 to the constants $G_\perp$ and $G_\vert$ by using $G_\vert S'^1_0 = G'^1_0$ and $G'^1_{\pm 1} = G_\perp S'^1_{\pm 1}$. With this we have

$$G_\vert = 2\langle \tfrac{1}{2} \vert G'^1_0 \vert \tfrac{1}{2}\rangle = -2\langle -\tfrac{1}{2} \vert G'^1_0 \vert -\tfrac{1}{2}\rangle, \tag{A11}$$

$$G_\perp = \sqrt{2}\langle -\tfrac{1}{2} \vert G'^1_{-1} \vert \tfrac{1}{2}\rangle = -\sqrt{2}\langle \tfrac{1}{2} \vert G'^1_{+1} \vert -\tfrac{1}{2}\rangle. \tag{A12}$$

$G_\vert$ and $G_\perp$ can be written in terms of the expansion coefficients of the unpaired electron [Eq. (A6)]:

$$G_\vert = \begin{cases} \sum_{\ell=0}^{\infty} \left[g\left(\left\vert c_0^\ell \right\vert^2 - \left\vert c_1^\ell \right\vert^2\right) + 2\left\vert c_1^\ell \right\vert^2 \right] \\ g \qquad \text{for a } \sigma \text{ orbital} \\ 2 - g \qquad \text{for a } \pi \text{ orbital,} \end{cases} \tag{A13}$$

$$G_\perp = \begin{cases} \sum_{\ell=0}^{\infty} \left[\left\vert c_0^\ell \right\vert^2 g + \sqrt{\ell(\ell+1)} \left\vert c_1^{\ell *} c_0^1 \right\vert \right] \\ g \qquad \text{for a } \sigma \text{ orbital} \\ 0 \qquad \text{for a } \pi \text{ orbital.} \end{cases} \tag{A14}$$

Again, angular momentum algebra can be used to find the Zeeman interaction with the result:

$$\begin{aligned} &\mu_B \langle F' J' I' M' p'_s \vert \sum_t (-1)^t G'^1_t B'^{1\prime}_{-t} \vert F J I M p_s \rangle \\ &= \mu_B \delta_{pp'} \delta_{II'} \sqrt{(2F+1)(2F'+1)(2J+1)(2J'+1)} \\ &\quad \times \frac{(-1)^{I+F'+J'}}{2} \begin{Bmatrix} J' & F' & I \\ F & J & 1 \end{Bmatrix} \left(\frac{1}{J_< + 1} + \frac{\delta_{JJ'}}{J} \right)^{1/2} \\ &\quad \times \left[\left(J' - J - \frac{\delta_{JJ'}}{2J+1} \right) \frac{G_\vert}{2} - p_s (-1)^{J-1/2} \frac{G_\perp}{2} \right] \\ &\quad \times B^1_{M-M'} (-1)^{F'-M} \begin{pmatrix} F' & 1 & F \\ -M' & M'-M & M \end{pmatrix}. \end{aligned} \tag{A15}$$

TABLE IX. Matrix elements of the hyperfine interaction $\mathbf{H}_1$ for the case $I_1 = I_2 = \frac{1}{2}$. Conjugate matrix elements given trivially by the Hermitian property of $\mathbf{H}_1$ are not shown.

$\langle F J' I' M p_s \vert \mathbf{H}_1 \vert F J I M p_s \rangle$			
$I = 0$ $J = F$	$I = 1$ $J = F$	$I = 1$ $J = F + 1$	$I=1$ $J = F - 1$
0	$-\sqrt{F(F+1)}\underline{c}_\chi$ $-\frac{(2F+3)(2F-1)}{8F(F+1)}t_0 - \bar{c}_\chi$	0 $\frac{3}{8F}\sqrt{\frac{(2F+3)F}{(F+1)^2}}t_0$ $\frac{(2F+5)}{8(F+1)}t_0 - (F+2)\bar{c}_\chi$	0 $-\frac{3}{8F}\sqrt{\frac{(2F-1)}{(F+1)}}t_0$ $-\frac{3}{8}\sqrt{\frac{(2F-1)(2F+3)}{F(F+1)}}t_0$ $\frac{(2F-3)}{8F}t_0 + (F-1)\bar{c}_\chi$
$\underline{c}_\chi = \frac{c_1 - c_2}{2} + p_s \frac{d_{c_1} - d_{c_2}}{4}(-1)^{J-1/2}(J+\frac{1}{2})$ $\bar{c}_\chi = \frac{c_1 + c_2}{2} + p_s \frac{d_{c_1} + d_{c_2}}{4}(-1)^{J-1/2}(J+\frac{1}{2})$			

Here $J_> = \max(J, J')$. Analysis of the nuclear Zeeman leads to the matrix elements

$$\begin{aligned}(-\mu_N)\langle F'J'I'p_s'M_s\|(g_1\mathbf{B}\cdot\mathbf{I}_1 + g_2\mathbf{B}\cdot\mathbf{I}_2)\|FJIp_sM_s\rangle \\ = (-1)^{I'+J+F+1}\sqrt{(2F'+1)(2F+1)}\begin{Bmatrix} I' & F' & J \\ F & I & 1\end{Bmatrix} \\ \times\Bigg(\Bigg[\bar{g}\sqrt{I(I+1)(2I+1)} \\ +\underline{g}\frac{(I_1-I_2)(I_1+I_2+1)(2I+1)}{\sqrt{I(I+1)(2I+1)}}\Bigg]\delta_{I,I'} + \underline{g}(I'-I) \\ \times\left[\frac{[I_>^2-(I_1-I_2)^2][(I_1+I_2+1)^2-I_>^2]}{I_>}\right]^{1/2}\delta_{|I-I'|,1}\Bigg) \\ \times B^1_{M-M'}(-1)^{F'-M}\begin{pmatrix} F' & 1 & F \\ -M' & M'-M & M\end{pmatrix}, \qquad \text{(A16)}\end{aligned}$$

where $I_> = \max(I, I')$

$$\bar{g} = \frac{g_1+g_2}{2}, \qquad \text{(A17)}$$

and

$$\underline{g} = \frac{g_1-g_1}{2}. \qquad \text{(A18)}$$

4. Stark interaction and dipole transition moments

We first consider the molecular frame expectation value of $\vec{r}'$. To do so we let

$$d^1_0 = z', \qquad \text{(A19)}$$

and

$$d^1_{\pm1} = \mp\frac{1}{\sqrt{2}}(x' \mp iy'). \qquad \text{(A20)}$$

Parity arguments may be used to show that

$$\left\langle\tfrac{1}{2}\middle|d^1_0\middle|\tfrac{1}{2}\right\rangle = \left\langle-\tfrac{1}{2}\middle|d^1_0\middle|-\tfrac{1}{2}\right\rangle = \alpha_z, \qquad \text{(A21)}$$

$$\left\langle\tfrac{1}{2}\middle|d^1_1\middle|-\tfrac{1}{2}\right\rangle = \left\langle-\tfrac{1}{2}\middle|d^1_{-1}\middle|\tfrac{1}{2}\right\rangle = \sqrt{2}\alpha_{xy}. \qquad \text{(A22)}$$

With these relationships, analysis of the matrix elements of

$$\begin{aligned}\langle F'J'I'M'p_s'|\vec{r}'\cdot\vec{E}|FJIMp_s\rangle \\ = \langle F'J'I'M'p_s'|\sum_t(-1)^t d'^1_{-t}E^{1}_t|FJIMp_s\rangle \qquad \text{(A23)}\end{aligned}$$

follows closely that of the Zeeman case, with

$$\begin{aligned}\langle F'J'I'M'p_s'|\sum_t(-1)^t r'^1_t E^{1}_{-t}|FJIMp_s\rangle \\ = \delta_{p_s,-p_s'}\delta_{II'}\sqrt{(2F+1)(2F'+1)(2J+1)(2J'+1)} \\ \times\frac{(-1)^{I+F'+J'}}{2}\begin{Bmatrix} J' & F' & I \\ F & J & 1\end{Bmatrix}\left(\frac{1}{J_<+1}+\frac{\delta_{JJ'}}{J}\right)^{1/2} \\ \times\left[\left(J'-J-\frac{\delta_{JJ'}}{2J+1}\right)\alpha_z + p_s(-1)^{J-1/2}\alpha_{xy}\right] \\ \times E^1_{M-M'}(-1)^{F'-M}\begin{pmatrix} F' & 1 & F \\ -M' & M'-M & M\end{pmatrix}. \qquad \text{(A24)}\end{aligned}$$

If α_z and α_{xy} are taken to be the body-fixed parallel and perpendicular transition dipole moments, then this matrix element gives the rotational-state dependence of the transition dipole moment. With the substitutions $\alpha_{xy} = 0$ and $\alpha_z = -d$ where d is the dipole moment of the molecule, Eq. (A24) becomes matrix elements describing the Stark interaction.

[1] E. Purcell and N. Ramsey, Phys. Rev. **78**, 807 (1950).
[2] E. D. Commins, S. B. Ross, D. DeMille, and B. C. Regan, Phys. Rev. A **50**, 2960 (1994).
[3] D. DeMille, F. Bay, S. Bickman, D. Kawall, D. Krause Jr, S. E. Maxwell, and L. R. Hunter, Phys. Rev. A **61**, 52507 (2000).
[4] J. J. Hudson, B. E. Sauer, M. R. Tarbutt, and E. A. Hinds, Phys. Rev. Lett. **89**, 23003 (2002).
[5] L. Sinclair, J. Bohn, A. Leanhardt, E. Meyer, R. Stutz, and E. Cornell, Bull. Am. Phys. Soc., 2007 APS March Meeting, Vol. 52, No. 1, 21.15E, 2007.
[6] J. Lee, R. Paudel, and A. Leanhardt, in Proceedings of the 21st International Conference on Atomic Physics, ICAP 2008.
[7] A. C. Vutha, O. K. Baker, W. C. Campbell, D. DeMille, J. M. Doyle, G. Gabrielse, Y. V. Gurevich, and M. A. Jansen, Bull. Am. Phys. Soc., 39th Annual Meeting of the APS Division of Atomic, Molecular, and Optical Physics, Vol. 53, No. 7, C5.000006, 2008.
[8] S. Bickman, P. Hamilton, Y. Jiang, and D. DeMille, Phys. Rev. A **80**, 023418 (2009).
[9] M. Kozlov, V. Fomichev, Y. Y. Dmitriev, L. Labzovsky, and A. Titov, J. Phys. B **20**, 4939 (1987).
[10] Y. Y. Dmitriev, Y. G. Khait, M. Kozlov, L. Labzovsky, A. Mitrushenkov, A. Shtoff, and A. Titov, Phys. Lett. A **167**, 280 (1992).
[11] N. E. Shafer-Ray, Phys. Rev. A **73**, 34102 (2006).
[12] C. P. McRaven, P. Sivakumar, and N. E. Shafer-Ray, Phys. Rev. A **75**, 024502 (2007).
[13] C. P. McRaven, P. Sivakumar, and N. E. Shafer-Ray, Phys. Rev. A **78**, 54502 (2008).
[14] M. Rupasinghe and N. E. Shafer-Ray, Phys. Rev. A **78**, 33427 (2008).
[15] P. Sivakumar, C. P. McRaven, D. Combs, N. E. Shafer-Ray, and V. Ezhov, Phys. Rev. A **77**, 62508 (2008).
[16] L. D. Alphei *et al.*, Phys. Rev. A **83**, 040501(R) (2011).
[17] D. Miller, *Atomic and Molecular Beam Methods* (Oxford University, Oxford, 1988), Vol. 1, p. 14.
[18] D. Banser, M. Schnell, J.-U. Grabow, E. J. Cocinero, A. Lesarri, and J. L. Alonso, Angew. Chem. **44**, 6311 (2005).
[19] B. M. Giuliano, L. Bizzocchi, and J.-U. Grabow, J. Mol. Spectrosc. **251**, 261 (2008).
[20] T. J. Balle and W. H. Flygare, Rev. Sci. Instrum. **52**, 33 (1981).
[21] J.-U. Grabow and W. Stahl, Z. Naturforsch. A **45**, 1043 (1990).
[22] J.-U. Grabow, W. Stahl, and H. Dreizler, Rev. Sci. Instrum. **67**, 4072 (1996).
[23] J.-U. Grabow and W. Caminati, *Frontiers of Molecular Spectroscopy* (Elsevier, Amsterdam, 2009), p. 383.
[24] J.-U. Grabow, *Handbook of High Resolution Spectroscopy* (Wiley, New York, 2011).

[25] P. Sivakumar, C. P. McRaven, P. M. Rupasinghe, T. Z. Yang, N. E. Shafer-Ray, T. J. Sears, and G. E. Hall, Mol. Phys. **108**, 927 (2010).
[26] J. M. Brown, E. A. Colbourn, J. K. G. Watson, and F. D. Wayne, J. Mol. Spectrosc. **74**, 294 (1979).
[27] C. Amiot, J. P. Maillard, and J. Chauville, J. Mol. Spectrosc. **87**, 196 (1981).
[28] K. Ziebarth, K. Setzer, O. Shestakov, and E. Fink, J. Mol. Spectrosc. **191**, 108 (1998).
[29] R. Frosch and H. Foley, Phys. Rev. **88**, 1337 (1952).
[30] J. M. Brown and A. Carrington, *Rotational Spectroscopy of Diatomic Molecules* (Cambridge University, Cambridge, England, 2003).
[31] *CRC Handbook of Chemistry and Physics*, 90th ed. (CRC Press, Boca Raton, FL, 2008).
[32] I. Kopp and J. Hougen, Can. J. Phys. **45**, 2581 (1967).
[33] K. I. Baklanov, A. N. Petrov, A. V. Titov, and M. G. Kozlov, Phys. Rev. A **82**, 060501 (2010).
[34] P. Rupasinghe, Ph.D. thesis, University of Oklahoma, 2010.
[35] A. Baum, B.S. thesis, Pomona College, 2010.
[36] D. Lumley and R. Barrow, J. Phys. B **10**, 1537 (1977).
[37] R. Zare, *Angular Momentum, Understanding Spatial Aspects in Chemistry and Physics* (Wiley Interscience, New York, 1988).